

Six heterometallic coordination polymers containing cobalt(II): Syntheses, crystal structures and magnetic properties



Ya-Qiu Sun^{a,*}, Shang-Yuan Liu^a, Yan-Yan Xu^a, Lin Wu^a, Dong-Zhao Gao^a, Guo-Ying Zhang^a, Dai-Zheng Liao^b

^aTianjin Key Laboratory of Structure and Performance for Functional Molecules, Key Laboratory of Inorganic–Organic Hybrid Functional Material Chemistry, Ministry of Education, College of Chemistry, Tianjin Normal University, Tianjin 300387, PR China

^bDepartment of Chemistry, Nankai University, Tianjin 300071, PR China

ARTICLE INFO

Article history:

Received 2 December 2013

Accepted 13 February 2014

Available online 5 March 2014

Keywords:

Coordination polymers

Heterometallic complex

Magnetism

Macrocylic oxamide complex

ABSTRACT

Six new coordination polymers, [Co(NiL)(aibt)] (**1**), [Co₂(ML)(hipt)₂(CH₃OH)(H₂O)]·CH₃OH (M = Cu (**2**), Ni (**3**)), [Co₂(C₂O₄)₂(CuL)₂] (**4**), [Co₄(NiL)₄(ipt)₄(H₂O)₂] (**5**) and [Co(CuL)(tpt)] (**6**) (H₂L = 2,3-dioxo-5,6,14,15-dibenzo-1,4,8,12-tetraazacyclo-pentadeca-7,13-dien; H₂aibt = 5-aminoisophthalic acid; H₂hipt = 5-hydroxyisophthalic acid; H₂ipt = isophthalic acid; H₂tpt = terephthalic acid), have been synthesized by a solvothermal method and characterized by single-crystal X-ray diffraction. Complexes **1**, **4** and **5** exhibit different infinite chain structures formed by CoNi (**1**), Co₂Cu₂ (**4**), Co₄Ni₄ (**5**) units, respectively, via oxamide and diverse carboxylate bridges, while complexes **2**, **3** and **6** exhibit different two-dimensional network structures formed by Co₂M or Co₂M₂ units via oxamide and 5-hydroxyisophthalate or terephthalate bridges. The results of magnetic determination show weak antiferromagnetic interactions in **1–3** and **5–6**, and the spin–orbit coupling interaction of Co(II) is a primary factor in the magnetic behaviors.

© 2014 Elsevier Ltd. All rights reserved.

1. Introduction

Coordination polymers have recently attracted much attention because of their fascinating structures and their potential application in magnetism, luminescence, adsorption, catalysis, etc. [1–6]. However, heterometallic coordination polymers, which often exhibit novel electromagnetic properties, remain relatively scarce because of the coordinative complexity of the heterometallic ions involved in the self-assembly process [7,8]. Recently, in order to design and construct diverse oxamido-bridged heteropolynuclear networks, we have chosen aromatic multicarboxylate ligands as co-ligands. The results show that the marrying of the ML macrocyclic units with aromatic multicarboxylate ligands have indeed led to novel and interesting one-dimensional, two-dimensional and three-dimensional extended networks [9–12]. In the majority of the coordination polymers, macrocyclic oxamide complexes, ML, were used as terminal ligands, which allowed us to synthesize one and two-dimensional heterobimetallic systems in a more controlled fashion [9–12]. Up to date, only the [Cd(HBTC)(CuL)]·H₂O three-dimensional network with the **sra** topology has been

synthesized. The results reported here and previously reported clearly show that solvothermal synthesis is a powerful and versatile tool for preparing macrocyclic oxamide and organic acid bridged coordination polymers [9–12].

On the other hand, the field of metal complex-based magnetic materials has made great achievements in the last two decades [13,14]. Especially, those containing cobalt(II) ions have received particular attention because of the special magnetic properties of Co(II) [15,16]. In an octahedral field, a single Co(II) ion has a ⁴T_{1g} ground state and magnetic behavior with a strong orbital contribution at high temperature (especially above 77 K). However, the Co(II) center in real chemical systems do not display a strict octahedral environment. In distorted octahedral systems, the degeneracy of the ⁴T_{1g} state is lifted. If the distortion is tetragonal, the ground state becomes ⁴A_{2g} and the excited level is ⁴E_g. Spin–orbit coupling in these levels results in six Kramer's doublets, with an *M* = ±1/2 ground state and an *M* = ±3/2 first excited state. The orbital moment has then been incorporated, in part, into the ZFS. Hence, the ZFS is much larger than for a metal ion with a quartet ground state and no first order orbital moment, such as Cr(III). Therefore, the advantage of using Co(II) to generate a large magnetic anisotropy is obvious. The large magnetic anisotropy would favor the production of slow magnetic relaxation effects, which are so-called single-molecule magnets (SMMs) and single chain

* Corresponding author. Tel.: +86 022 23503778.

E-mail addresses: hxyxyq@mail.tjnu.edu.cn (Y.-Q. Sun), liao dz@nankai.edu.cn (D.-Z. Liao).

magnets (SCMs). To date, many complexes containing the high-spin Co(II) ion are SMMs and SCMs [17–21]. Moreover, from a theoretical point of view, the magnetic exchange in polynuclear complexes containing six-coordinated Co(II) ions is a challenging subject because of the orbital angular momentum cause in the theoretical analysis of the magnetic data.

In this paper, in order to study the magnetic properties of heterometallic coordination polymers with larger magnetic anisotropies, we chose 5-aminoisophthalate, 5-hydroxyisophthalate, isophthalate, terephthalate and ML macrocyclic units as potential bridging ligands to react with Co²⁺ metal ions. Three different types of one-dimensional and three two-dimensional coordination polymers were firstly obtained and used an approximate model to estimate the magnetic exchange and spin–orbital interactions for these complexes.

2. Experimental

2.1. Materials and physical measurements

All the starting reagents were of A. R. grade and were used as purchased. The complex ligand ML (M = Cu, Ni) was prepared as described elsewhere [22]. Analyses of C, H and N were determined on a Perkin-Elmer 240 Elemental analyzer. The IR spectra were recorded using the KBr disc technique on a Shimadzu IR-408 infrared spectrophotometer in the 4000–600 cm⁻¹ range. X-ray powder diffraction (XRPD) spectra for the powders were recorded on a Model D/MAX-2550 V diffractometer (Rigaku, Japan). Variable-temperature magnetic susceptibilities were measured on an MPMS-7 SQUID magnetometer. Diamagnetic corrections were made with Pascal's constants for all the constituent atoms [23].

2.2. X-ray crystallography

Single crystal X-ray diffraction analyses of **1–6** were carried out on a Bruker Smart Apex II CCD diffractometer equipped with graphite monochromated Mo K α radiation ($\lambda = 0.71073 \text{ \AA}$) using the ϕ/ω scan technique at room temperature. Semi-empirical absorption corrections were applied using SADABS. All structures were solved by direct methods using the SHELXS program of the SHELXTL package and refined with SHELXL. The crystallographic data and selected bond lengths for **1–6** are listed in Tables 1 and 2.

2.3. Preparation of complexes of **1–6**

2.3.1. Synthesis of [Co(NiL)(aipt)] (**1**)

A mixture of Co(Ac)₂·6H₂O (0.10 mmol), H₂aipt (0.05 mmol), NiL (0.05 mmol), H₂O (10 mL) and CH₃OH (4 mL) was stirred for 30 min at room temperature and the pH value of the solution was adjusted to about 7–8 with triethylamine (0.01 mmol). The mixture was transferred to an 18 mL Teflon-lined reactor, heated to 150 °C over 24 h and then kept at 150 °C for 72 h. Finally, the reaction system was cooled to room temperature over 36 h, and deep brown–red crystals of **1** were obtained (yield 37.5% based on Co). *Anal. Calc.* for C₂₇H₂₁CoN₅NiO₆ **1**: C, 51.50; H, 3.34; N, 11.13. Found: C, 51.46; H, 3.33; N, 11.08%. Main IR bands (KBr, cm⁻¹): 3417 (w, N–H), 1627 (s, C=O, COO⁻), 1605 (s, C=O, oxamide), 1563 (s, C=N).

2.3.2. Synthesis of [Co₂(ML)(hipt)₂(CH₃OH)(H₂O)]·CH₃OH (M = Cu (**2**), Ni (**3**))

A mixture of Co(Ac)₂·6H₂O (0.1 mmol), H₂hipt (0.05 mmol), ML (0.05 mmol), H₂O (10 mL) and CH₃OH (4 mL) was stirred for 30 min at room temperature and the pH value of the solution was adjusted to about 7–8 with triethylamine (0.01 mmol). The

mixture was transferred to an 18 mL Teflon-lined reactor, heated to 150 °C over 24 h and then kept at 150 °C for 72 h. Finally, the reaction system was cooled to room temperature over 36 h, and deep brown crystals of compound **2** and red crystals of compound **3** were isolated by filtering and washing with water. *Anal. Calc.* for C₃₇H₃₄Co₂CuN₄O₁₅ **2**: C, 46.44; H, 3.56; N, 5.86. Found: C, 46.47; H, 3.58; N, 5.89%. Main IR bands, cm⁻¹: 3429 (m(br), O–H), 1642 (m, C=O, COO⁻), 1613 (m, C=O, oxamide), 1554 (s, C=N). *Anal. Calc.* for C₃₇H₃₄Co₂N₄NiO₁₅ **3**: C, 46.68; H, 3.57; N, 5.89. Found: C, 46.66; H, 3.55; N, 5.85%. Main IR bands, cm⁻¹: 3423 (m(br), O–H), 1642 (m, C=O, COO⁻), 1610 (m, C=O, oxamide), 1551 (s, C=N).

2.3.3. Synthesis of [Co₂(C₂O₄)₂(CuL)₂] (**4**)

A mixture of Co(Ac)₂·6H₂O (0.1 mmol), 2-aminoterephthalic acid (0.05 mmol), CuL (0.05 mmol), H₂O (10 mL) and CH₃OH (4 mL) was stirred for 40 min at room temperature, and the pH value of the solution was adjusted to about 8–9 with triethylamine (0.01 mmol). The mixture was transferred to an 18 mL Teflon-lined reactor, heated to 150 °C over 24 h and then kept at 150 °C for 72 h. Finally, the reaction system was cooled to room temperature over 36 h, and deep brown–green crystals of compound **4** were isolated (yield 38.5% based on Co) by filtering and washing with water. *Anal. Calc.* for C₈₄H₆₄Co₄Cu₄N₁₆O₂₄ **4**: C, 46.42; H, 2.95; N, 10.32. Found: C, 46.44; H, 2.93; N, 10.35%. Main IR bands: 1647 (s, C=O, COO⁻), 1611 (s, C=O, oxamide), 1563 (s, C=N).

2.3.4. Synthesis of [Co₄(NiL)₄(ipt)₄(H₂O)₂] (**5**)

A mixture of Co(Ac)₂·6H₂O (0.05 mmol), H₂ipt (0.05 mmol), NiL (0.025 mmol), H₂O (10 mL) and CH₃OH (4 mL) was stirred for 30 min at room temperature, and the pH value of the solution was adjusted to about 7–8 with triethylamine (0.01 mmol). The mixture was transferred to an 18 mL Teflon-lined reactor, heated to 150 °C over 24 h and then kept at 150 °C for 72 h. Finally, the reaction system was cooled to room temperature over 36 h, and deep brown–red crystals of compound **5** were isolated (yield 45.3% based on Co). *Anal. Calc.* for C₁₀₈H₈₄Co₄N₁₆Ni₄O₂₆ **5**: C, 52.00; H, 3.37; N, 8.99. Found: C, 52.00; H, 3.39; N, 9.01%. Main IR bands, cm⁻¹: 3416 (s(br), O–H), 1630 (s, C=O, COO⁻), 1604 (s, C=O, oxamide), 1564 (s, C=N).

2.3.5. Synthesis of [Co(CuL)(tpt)] (**6**)

A mixture of Co(Ac)₂·6H₂O (0.05 mmol), H₂tpt (0.05 mmol), CuL (0.025 mmol), H₂O (10 mL) and CH₃OH (4 mL) was stirred for 30 min at room temperature, and the pH value of the solution was adjusted to about 7–8 with triethylamine (0.01 mmol). The mixture was transferred to an 18 mL Teflon-lined reactor, heated to 150 °C over 24 h and then kept at 150 °C for 72 h. Finally, the reaction system was cooled to room temperature over 36 h, and deep brown–green crystals of compound **6** were isolated (yield 65.4% based on Co). *Anal. Calc.* for C₂₇H₂₀CoCuN₄O₆ **6**: C, 52.35; H, 3.23; N, 9.05. Found: C, 52.38; H, 3.27; N, 9.03%. Main IR bands, cm⁻¹: 1637 (s, C=O, COO⁻), 1603 (s, C=O, oxamide), 1584 (s, C=N).

3. Results and discussion

3.1. Synthetic and spectral aspects

By using 5-aminoisophthalate, 5-hydroxyisophthalate, isophthalate or terephthalate and macrocyclic oxamide mixed ligands as the metal linker, the coordination polymers **1–6** were obtained in the same mixed-solvent systems, with the same times and temperature under solvothermal conditions. Complexes **1, 2, 3, 5** and **6** were obtained at pH 7–8, while compound **4** was obtained at a relatively higher pH 8–9, and the oxalate group in the product arises from the hydrolysis of the oxamide ligand. Complexes **1–6** are

Table 1
Crystal data and structure refinement for complexes 1–6.

Complexes	1	2	3	4	5	6
Formula	C ₂₇ H ₂₁ CoN ₅ NiO ₆	C ₁₄₈ H ₁₃₆ Co ₈ Cu ₄ N ₁₆ O ₆₀	C ₃₇ H ₃₄ Co ₂ N ₄ NiO ₁₅	C ₈₄ H ₆₄ Co ₄ Cu ₄ N ₁₆ O ₂₄	C ₁₀₈ H ₈₄ Co ₄ N ₁₆ Ni ₄ O ₂₆	C ₂₇ H ₂₀ CoCuN ₄ O ₆
Formula weight	629.13	3824.33	951.25	2171.39	2492.47	618.94
Crystal system	triclinic	monoclinic	monoclinic	monoclinic	triclinic	triclinic
Space group	P $\bar{1}$	P2 ₁ /c	P2 ₁ /c	P2(1)/n	P $\bar{1}$	P $\bar{1}$
<i>a</i> (Å)	10.0384(8)	11.794(5)	12.039(5)	9.7954(10)	13.9971(6)	9.9613(8)
<i>b</i> (Å)	10.8925(8)	16.703(7)	16.306(6)	24.686(3)	17.0166(8)	12.0095(10)
<i>c</i> (Å)	11.9122(9)	18.492(7)	18.520(7)	15.9523(16)	22.1463(10)	12.2172(11)
α (°)	104.240(1)	90	90	90	82.0440(10)	68.5910(10)
β (°)	97.433(1)	94.184(7)	94.551(6)	92.175(2)	73.2060(10)	85.854(2)
γ (°)	101.425(1)	90	90	90	86.3070(10)	67.7730(10)
<i>V</i> (Å ³)	1215.5(2)	3633(3)	3624(2)	3854.6(7)	4999.6(4)	1255.91(18)
<i>Z</i>	2	1	4	2	2	2
<i>r</i> _{calc.} (g cm ⁻³)	1.719	1.748	1.743	1.871	1.656	1.637
<i>v</i> (Mo K α) (mm ⁻¹)	0.71073	0.71073	0.71073	0.71073	0.71073	0.71073
Crystal size (mm)	0.20 × 0.19 × 0.18	0.18 × 0.16 × 0.15	0.18 × 0.16 × 0.14	0.15 × 0.14 × 0.12	0.17 × 0.16 × 0.12	0.18 × 0.17 × 0.16
<i>T</i> (K)	296(2)	296(2)	173(2)	173(2)	296(2)	296(2)
Goodness-of-fit <i>F</i> ²	1.034	1.048	1.018	1.023	1.005	1.051
Reflections collected/unique	25039/4835	18042/6392	17815/6383	19550/6787	25917/17536	6523/4403
<i>R</i> _{int}	0.0096	0.0423	0.1180	0.0572	0.0293	0.0170
<i>R</i> ₁ ^a [<i>I</i> > 2 σ (<i>I</i>)]	0.0234	0.0378	0.0617	0.0418	0.0433	0.0322
<i>wR</i> ₂ ^b [<i>I</i> > 2 σ (<i>I</i>)]	0.0639	0.0898	0.1293	0.0914	0.0757	0.0778
<i>R</i> ₁ ^a [all data]	0.0256	0.0628	0.1215	0.0715	0.0837	0.0402
<i>wR</i> ₂ ^b [all data]	0.0655	0.1027	0.1562	0.1053	0.0892	0.0820

^a $R_1 = \sum ||F_o| - |F_c|| / \sum |F_o|$.^b $wR_2 = \{ \sum [w(F_o^2 - F_c^2)]^2 / \sum [w(F_o^2)]^2 \}^{1/2}$.**Table 2**
Selected bond distances (Å) for 1–6.

Compound 1			
Ni(1)–N(1)	1.879(2)	Ni(1)–N(4)	1.894(1)
Co(1)–O(4)#1	2.007(1)	Co(1)–O(3)	2.079(9)
Co(1)–O(5)#2	2.136(1)	Co(1)–O(1)	2.216(1)
Compound 2			
Cu(1)–N(3)	1.871(3)	Cu(1)–N(4)	1.897(3)
Co(1)–O(4)	2.008(3)	Co(1)–O(8)	2.239(3)
Co(2)–O(11)#2	2.051(3)	Co(2)–O(8)	2.182(3)
Compound 3			
Ni(1)–N(4)	1.926(5)	Ni(1)–N(1)	1.948(5)
Co(1)–O(3)	2.012(5)	Co(1)–O(9)	2.297(5)
Co(2)–O(4)	2.079(5)	Co(2)–O(9)	2.220(5)
Compound 4			
Cu(1)–N(4)	1.972(4)	Cu(1)–N(3)	2.004(4)
Cu(2)–N(5)	1.988(4)	Cu(2)–N(7)	2.012(4)
Co(1)–O(11)	2.058(3)	Co(1)–O(3)	2.161(3)
Co(2)–O(6)	2.052(3)	Co(2)–O(1)	2.164(3)
Compound 5			
Ni(1)–N(3)	1.864(3)	Ni(1)–N(4)	1.904(3)
Ni(2)–N(7)	1.867(3)	Ni(2)–N(5)	1.897(3)
Ni(3)–N(11)	1.868(3)	Ni(3)–N(12)	1.890(3)
Ni(4)–N(15)	1.872(3)	Ni(4)–N(13)	1.903(3)
Co(1)–O(13)	2.037(2)	Co(1)–O(10)	2.247(3)
Co(2)–O(12)#1	1.978(3)	Co(2)–O(17)	2.295(3)
Co(3)–O(5)	2.122(2)	Co(3)–O(16)	2.392(3)
Co(4)–O(19)#2	2.030(2)	Co(4)–O(23)	2.335(3)
Compound 6			
Co(1)–O(5)	2.025(18)	Co(1)–O(3)	2.176(2)
Cu(1)–N(1)	1.930(2)	Cu(1)–N(2)	1.952(2)

Symmetry transformations: **1**: #1 $-x+2, -y+1, -z+2$; #2 $-x+1, -y+1, -z+2$. **2**: #2 $-x, -y+1, -z+1$. **5**: #1 $x+1, y, z$; #2 $x-1, y, z$.

stable under ambient conditions and insoluble in common solvents such as water, alcohol and acetonitrile. The crystalline phase purity of **1**, **5** and **6** was confirmed by their experimental XRPD patterns, which match well with the corresponding simulated ones obtained from the single-crystal data (Fig. S1).

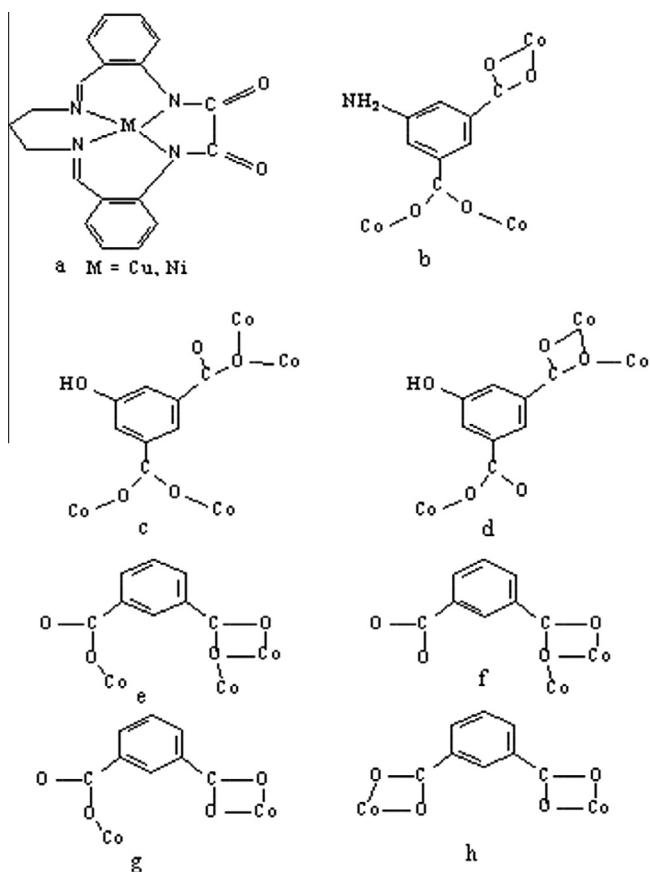
For complexes **1–6**, the IR spectra exhibit strong absorption bands in the regions 1647–1603 and 1584–1541 cm⁻¹ due to

$\nu(\text{C}=\text{O})$ and $\nu(\text{C}=\text{N})$ vibrations, respectively [24,25]. The IR spectra of **1–6** show no bands in the region 1680–1720 cm⁻¹, indicating complete deprotonation of the carboxyl groups. For complex **1**, the band around 3417 cm⁻¹ is characteristic of the NH₂ group [25]. For complexes **2**, **3** and **5**, the bands around 3416–3429 cm⁻¹ are characteristic of the hydroxyl group from H₂O and/or CH₃OH.

3.2. Structural description

The ligands involved in this research and the coordination modes of the aromatic multicarboxylates are listed in Scheme 1. Single-crystal X-ray analysis revealed that complex **1** is an infinite chain coordination polymer composed of tetranuclear Co₂Ni₂ building units. As shown in Fig. 1a, in the tetranuclear structure of **1**, the nickel ion is coordinated by four nitrogen atoms from the macrocyclic organic ligand, with the [NiN₄] geometry exhibiting distorted square planarity. The Co1 center is six-coordinated by two oxygen atoms from one oxamido ligand (Co1–O1 = 2.215(1) and Co1–O2 = 2.075(1) Å) and four oxygen atoms belonging to three different carboxylate groups from three separated aipt²⁻ ligands (the Co–O bond lengths range from 2.007(1) to 2.208(1) Å). The adjacent Co1 and Co1A centers are connected by two carboxylate groups from two aipt²⁻ ligands, adopting a bridging mode to construct a binuclear [Co₂(CO₂)₂] unit, in which the non-bonding Co···Co distance is 4.133(2) Å. Nickel ions and [Co₂(CO₂)₂] units are interlinked through the macrocyclic oxamide ligand to form a heterotetranuclear Co₂Ni₂ unit. The structural Co₂Ni₂ building units are further linked with each other through the aipt²⁻ ligand to create an infinite double chain. In the infinite chain structure, each aipt²⁻ ligand connects three cobalt ions with carboxylate groups, adopting chelating and bridging coordination modes, as shown in Scheme 1b and Fig. 1b. Furthermore, the 1D infinite chains are linked together by N–H···O hydrogen bonding to form a 2D framework. The *d* (H···O) and *d* (N···O) distances between the chains are 2.13 and 3.0153 Å, respectively.

Compounds **2** and **3** are isostructural, hence only the structure of **2** will be discussed in detail as a representative example. The asymmetric unit of **2** consists of two cobalt(II) ions, one copper(II) ion, one macrocyclic oxamide group, two hipt²⁻ ligands, two



Scheme 1. (a) The macrocylic oxamide complex ligands (ML). (b) The coordination modes of 5-aminoisophthalate (aipt²⁻). (c and d) The coordinated modes of 5-hydroxyisophthalate (hipt²⁻). (e–h) The coordinated modes of isophthalate (ipt²⁻).

CH₃OH and one water molecule. As shown in Fig. 2a, the Co1 center is linked to the Cu1 center via exo-cis oxygen donors of the macrocyclic oxamide ligand, in which the non-bonding Co1...Cu1 distance is 5.293(2) Å. The Cu1 center is coordinated by four nitrogen atoms from the macrocyclic organic ligand, with the [CuN₄] geometry exhibiting distorted square planarity. The Co1 center is six-coordinated by two oxygen atoms from one oxamide ligand and four carboxylate oxygen atoms from three different hipt²⁻ ligands. The coordination sphere of the Co1 center is a distorted octahedron, which can be seen from the O–Co–O bond angles, varying from 60.2(2)° to 173.1(2)°. The Co2 center coordinates with four carboxylate oxygen atoms from four different hipt²⁻ ligands, one oxygen atom from H₂O and one oxygen atom from CH₃OH, with a distorted octahedral [CoO₆] geometry (the Co–O bond lengths range from 2.073(5) to 2.220(5) Å). Adjacent Co1 and Co2 centers are connected by three carboxylate groups from three hipt²⁻ ligands to construct a binuclear [Co₂O₂] cluster, in which the non-bonding Co1...Co2 distance is 3.106(1) Å. Two asymmetric [Co₂Cu] units are connected by two hipt²⁻ ligands to construct a hexanuclear [Co₄Cu₂] unit (Fig. 2b). The hexanuclear [Co₄Cu₂] units are interlinked through bridging hipt²⁻ ligands to form a two-dimensional framework with nanometer pores, as shown in Fig. 2c. Each nanometer pore is composed of six [Co₂O₂] clusters, with a maximum Co...Co distance of 22.64 Å. In the two-dimensional framework, one kind of hipt²⁻ ligand connects four Co(II) ions using carboxylate groups, adopting two different bridging coordination modes (Scheme 1c), while another kind of hipt²⁻ ligand connects three Co(II) ions, with the

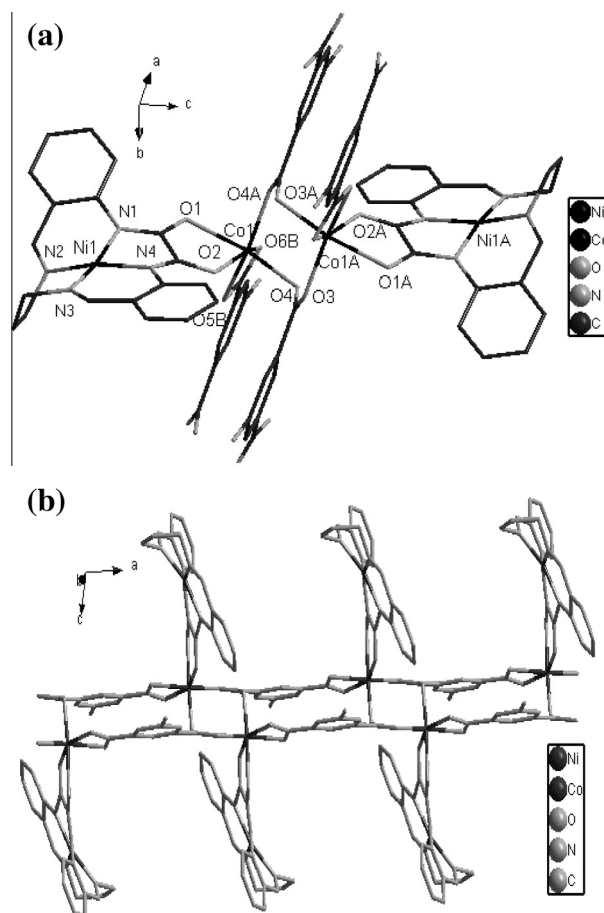


Fig. 1. (a) Perspective view of the Co₂Ni₂ unit (symmetry transformations used to generate equivalent atoms: A, 2–x, 1–y, 2–z; B, 1–x, 1–y, 2–z). (b) The polyhedral view of the self-assembled 1D double chain structure constructed by [Co₂(NiL)₂(aipt)₂].

carboxylate groups adopting monodentate and bridging coordination modes (see Scheme 1d).

Single-crystal X-ray analysis revealed that **4** is an infinite chain consisting of two crystallographic independent cobalt(II) ions and two crystallographic independent copper(II) ions. As shown in Fig. 3a, the Cu(II) ion is four-coordinated by four nitrogen atoms from the macrocyclic organic ligand, with Cu1–N distances in the range 1.972(4)–2.004(4) Å, to complete the distorted square planar coordination geometry. The Co(II) ion is six-coordinated by two oxygen atoms from one oxamide ligand, and four carboxylate oxygen atoms from two different C₂O₄²⁻ ligands, with a distorted octahedral [CoO₆] geometry. The Co1–O bond lengths range from 2.058(3) to 2.161(3) Å. Two adjacent cobalt(II) ions are connected by C₂O₄²⁻ ligands to construct a binuclear [Co₂] unit, in which the non-bonding Co...Co distance is 5.409(9) Å. Two Cu(II) ions and the [Co₂] unit are interlinked through the macrocyclic oxamide ligand to form a tetranuclear Cu₂Co₂ unit. Adjacent tetranuclear Cu₂Co₂ units are connected by bridging C₂O₄²⁻ ligands to form a one-dimensional zigzag framework (Fig. 3b). Furthermore, the 1D infinite chains are linked together by C–H...O hydrogen bonding to form a 2D framework. The *d* (H...O) and *d* (C...O) distances between the chains are 2.44 and 3.167 Å, respectively.

Single-crystal X-ray analysis revealed that **5** is a complicated one-dimensional ladder-like polymer consisting of four crystallographically independent cobalt(II) ions and four crystallographically independent nickel(II) ions. As shown in Fig. 4a, in the octanuclear structure of **5**, each Co(II) ion is linked to a Ni(II) ion via the exo-cis oxygen donors of the macrocyclic oxamide ligand

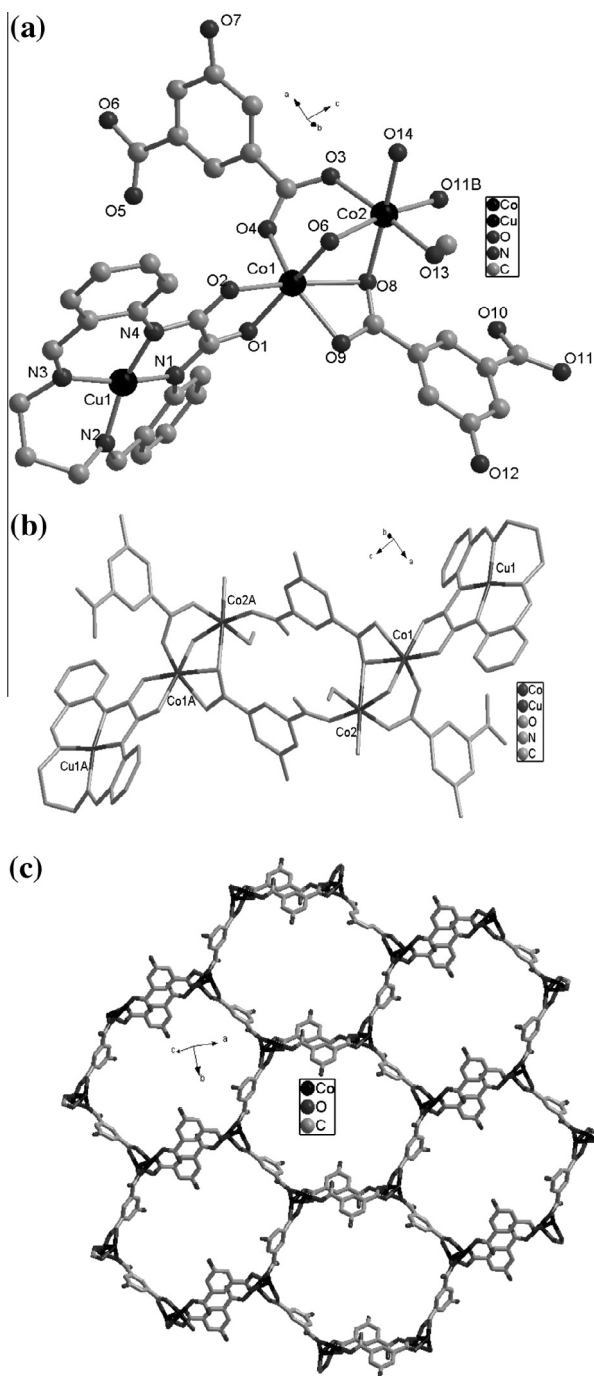


Fig. 2. (a) Perspective view of the Co_2Cu unit in **2**. (b) Perspective view of the Co_4Cu_2 unit in **2**. (c) View of the self-assembled 2D sheet structure constructed by $[\text{Co}_2(\text{CuL})(\text{hpt})_2(\text{CH}_3\text{OH})(\text{H}_2\text{O})_2]_2$; hydrogen atoms and CuL ligands are removed for clarity.

to form a $[\text{CoNi}]$ unit. The Ni(II) ion is coordinated by four nitrogen atoms from the macrocyclic organic ligand, with the $[\text{NiN}_4]$ geometry exhibiting distorted square planarity. The Co1 center has a distorted octahedral geometry with two oxygen atoms from one oxamido ligand, three carboxylate oxygen atoms from two different ipt^{2-} ligands and one oxygen atom from a water molecule. The Co1–O distances vary from 2.037(2) to 2.247(3) Å. The coordination environment of Co4 is the same as that of Co1. The Co2 ion also has a distorted octahedral geometry with two oxygen atoms from one oxamido ligand and four carboxylate oxygen atoms from

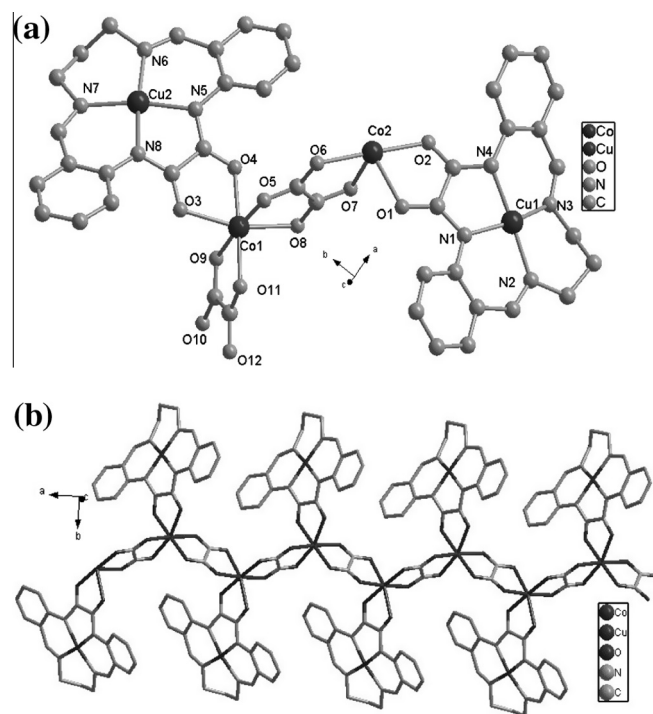


Fig. 3. (a) Portion of the crystal structure of **4** showing the coordination environments of the Co(II) and Cu(II) ions. (b) View of the self-assembled 1D chain structure constructed by $[\text{Co}_2(\text{C}_2\text{O}_4)_2(\text{CuL})_2]$; hydrogen atoms are removed for clarity.

three different ipt^{2-} ligands, while the Co3 ion is seven-coordinated by two oxygen atoms from one oxamido ligand and five carboxylate oxygen atoms from three different ipt^{2-} ligands, with the $[\text{CoO}_7]$ geometry exhibiting a distorted capped-octahedron. Two adjacent Ni_2Co_2 and Ni_3Co_3 units are connected by two carboxylate groups from two different ipt^{2-} ligands to construct a tetranuclear cluster, $[\text{Ni}_2\text{Co}_2\text{O}_2]$, in which the non-bonding $\text{Co}_2 \cdots \text{Co}_3$ distance is 3.416(9) Å. Two $[\text{CoNi}]$ units and one $[\text{Ni}_2\text{Co}_2\text{O}_2]$ cluster are interlinked through an ipt^{2-} ligand to form an octanuclear Co_4Ni_4 unit. Adjacent octanuclear Co_4Ni_4 units are connected by two bridging ipt^{2-} ligands to form a one-dimensional ladder-like chain (Fig. 4b). In the one-dimensional framework, the ipt^{2-} ligands have four coordination modes. The first kind of ipt^{2-} ligand connects three Co(II) ions with the carboxylate groups adopting monodentate and bridging coordination modes (Scheme 1e); the second kind of ipt^{2-} ligand connects two Co(II) ions with the carboxylate groups adopting tridentate bridging coordination modes (Scheme 1f); the third kind of ipt^{2-} ligand connects two Co(II) ions with the carboxylate groups adopting monodentate and bidentate-chelating coordination modes (Scheme 1g); and the last kind of ipt^{2-} ligand connects two Co(II) ions with the carboxylate groups adopting chelating coordination modes (Scheme 1h). Furthermore, the 1D infinite chains are linked together with $\text{O} \cdots \text{H} \cdots \text{O}$ hydrogen bonding to form a 2D framework. The $d(\text{H} \cdots \text{O})$ and $d(\text{O} \cdots \text{O})$ distances between the chains are 1.78–1.96 and 2.59–2.81 Å, respectively.

Single-crystal X-ray analysis revealed that complex **6** is a two-dimensional network coordination polymer constructed from a binuclear $[\text{Co}_2(\text{CO}_2)_2]$ unit, the macrocyclic oxamide CuL and tpt^{2-} linkers. As shown in Fig. 5a, the fundamental building unit for the crystal structure of **6** is composed of $[\text{Co}_2(\text{CuL})_2(\text{tpt})_2]$. The coordination geometry of the Cu(II) ion is slightly distorted square planar. The Co1 center is six-coordinated by two oxygen atoms from an oxamido ligand and four oxygen atoms belonging to three different

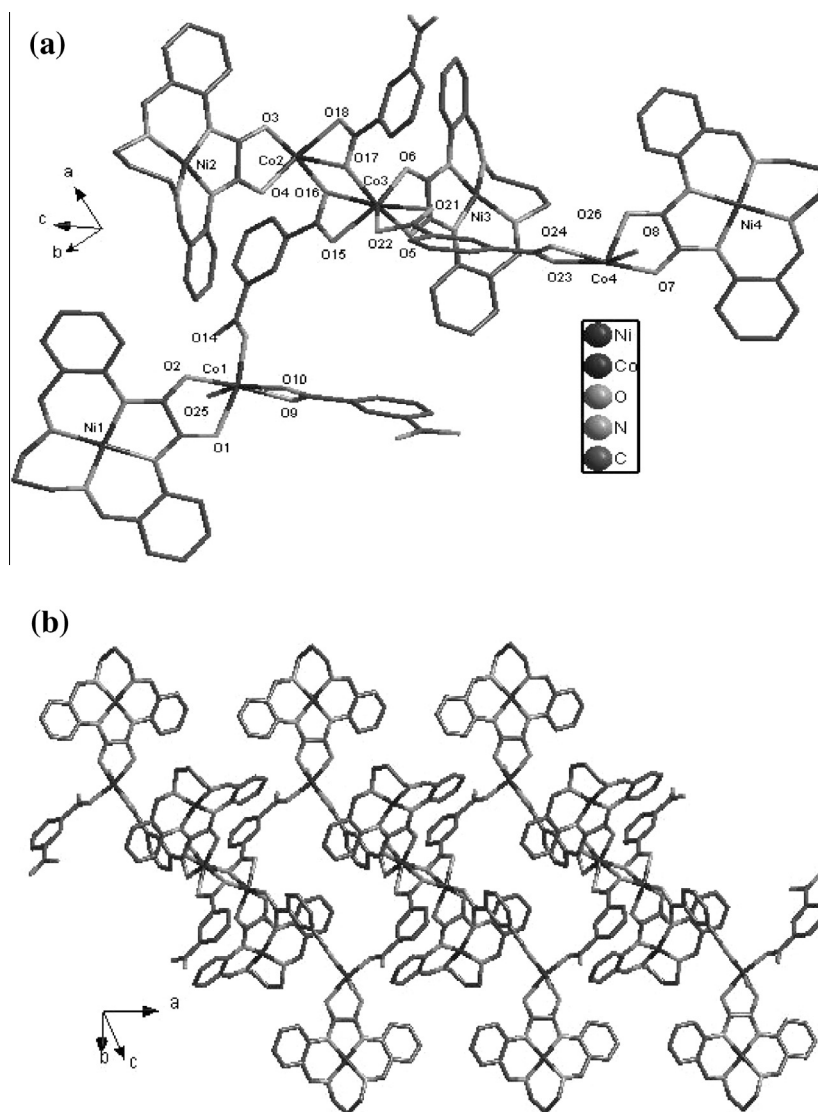


Fig. 4. (a) Perspective view of the Co_4Ni_4 unit in **5**. (b) View of the self-assembled 1D ladder-like structure constructed by $[\text{Co}_4(\text{NiL})_4(\text{ipt})_4(\text{H}_2\text{O})_2]$; hydrogen atoms are removed for clarity.

carboxylate groups from three separate tpt^{2-} ligands. The Co1-O distances vary from 2.024(2) to 2.176(2) Å. Two adjacent metal ions (Co1 and Co1A) are connected by two bridging $\mu_2\text{-COO}$ groups to construct a binuclear $[\text{Co}_2(\text{CO}_2)_2]$ unit, in which the non-bonding $\text{Co}\cdots\text{Co}$ distance is 4.381(5) Å. The copper ions and $[\text{Co}_2(\text{CO}_2)_2]$ units are interlinked through the macrocyclic oxamide ligand to form heterotetranuclear Cu_2Co_2 units. The Cu_2Co_2 units are further linked with each other through tpt^{2-} ligands to create a two-dimensional network (Fig. 5b). In the two-dimensional framework, one kind of tpt^{2-} ligand connects four Co(II) ions with the carboxylate groups adopting bridging coordination modes, and another kind of tpt^{2-} ligand connects two Co(II) ions with the carboxylate groups adopting chelating coordination modes. From a topological view of complex **6**, the two-dimensional network consists of Cu_2Co_2 SBUs, and each Cu_2Co_2 unit is connected through four carboxylate groups. Consequently, the Cu_2Co_2 unit can be viewed as a regular four-connected node. The tpt^{2-} ligand is a linear linker. Thus, polymer **6** has a uninodal 4-connected (4, 4) grid topology.

3.3. Magnetic properties

The magnetization measurements for complexes **1–3**, **5** and **6** have been carried out under 1 kOe. For these complexes, the

measured $\chi_M T$ values are all higher than the spin-only values at room temperature. This indicates an important contribution from the orbital momentum, typical for high-spin octahedral Co(II) with the $^4\text{T}_{1g}$ ground state. So the contribution of the spin-orbit coupling of the Co(II) ion was considered according to van Vleck's equation [26]. The value $\chi_M T = 6.58 \text{ cm}^3 \text{ mol}^{-1} \text{ K}$ at 300 K for a powder sample of **1** is larger than the spin-only value of $3.76 \text{ cm}^3 \text{ mol}^{-1} \text{ K}$ expected for the uncoupled Co_2^{II} binuclear system (Fig. S2). On lowering the temperature, $\chi_M T$ decreases continuously and reaches $2.31 \text{ cm}^3 \text{ mol}^{-1} \text{ K}$ at 2 K. On the basis of the crystal structure of **1** and the fact that the Ni^{II} ion is diamagnetic in the NiL subunit, the coupling topology deduced from the crystal structure has to be considered as the Co_2 binuclear unit. The magnetic analysis was carried out using the spin Hamiltonian: $\hat{H} = -2J\hat{S}_{\text{Co1}}\hat{S}_{\text{Co2}} + g_{\text{Co}}\beta H_Z\hat{S}_Z$ where J characterized the exchange interaction for Co-Co . The susceptibility of the binuclear unit CoCo , χ_{CoCo} , is calculated from Eq. (1):

$$\chi_{\text{CoCo}} = \frac{2N\beta^2 g_{\text{Co}}^2}{kT} \cdot \frac{A}{B} \quad (1)$$

$$A = 14 + 5 \exp(-6J/kT) + \exp(-10J/kT)$$

$$B = 7 + 5 \exp(-6J/kT) + 3 \exp(-10J/kT) + \exp(-12J/kT)$$

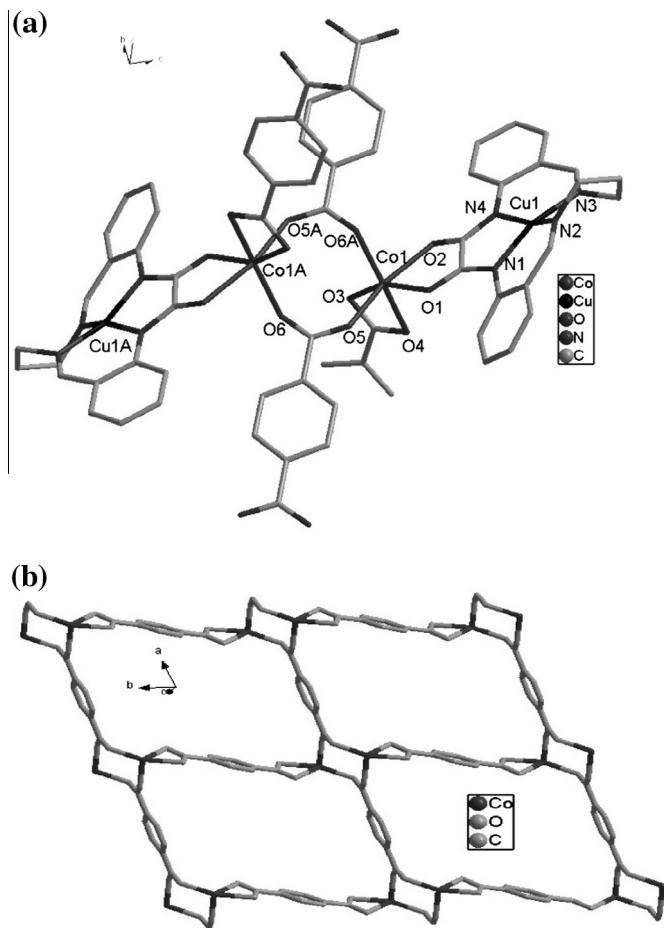


Fig. 5. (a) Perspective view of the Co_2Cu_2 unit in **6**. (b) The view of the self-assembled 2D sheet constructed by $[\text{Co}(\text{CuL})(\text{tpt})]$; hydrogen atoms and CuL ligands are removed for clarity.

where a part of the orbital angular momentum of the $\text{Co}(\text{II})$ ion is reflected in the temperature dependence of the g_{Co} factor (Eq. (2)) [27].

$$g_{\text{Co}} = \sqrt{\frac{3kT\chi_{\text{Co}}}{N\beta^2 S(S+1)}} \quad (2)$$

$$\chi_{\text{Co}} = \frac{N\beta^2 F_1}{3kT F_2}$$

$$F_1 = \frac{7\lambda(3-A)^2}{5kT} + \frac{12(2+A)^2}{25A} + \left[\frac{2\lambda(11-2A)^2}{45kT} + \frac{176(A+2)^2}{675A} \right] \exp\left(\frac{-5A\lambda}{2kT}\right) + \left[\frac{\lambda(A+5)^2}{9kT} - \frac{20(A+2)^2}{27A} \right] \exp\left(\frac{-4A\lambda}{kT}\right)$$

$$F_2 = \frac{\lambda}{3kT} \left[3 + 2 \exp\left(\frac{-5A\lambda}{2kT}\right) + \exp\left(\frac{-4A\lambda}{kT}\right) \right]$$

A is the ligand field parameter and λ is the spin–orbit coupling parameter. The least-squares fit to the experimental data was found with $J = -6.80 \times 10^{-3} \text{ cm}^{-1}$, $A = 1.49$ and $\lambda = -120$. R , the agreement factor defined as $R = \frac{\sum [(\chi_M)^{\text{Cal}} - (\chi_M)^{\text{obsd}}]^2}{\sum [(\chi_M)^{\text{obsd}}]^2}$, is 2.15×10^{-5} . The point below 14 K cannot be reproduced with this model.

For complex **2**, the χ_{MT} value is equal to $6.45 \text{ cm}^3 \text{ mol}^{-1} \text{ K}$ at 300 K, which is larger than the spin-only value ($4.12 \text{ cm}^3 \text{ mol}^{-1} \text{ K}$) expected for the uncoupled $\text{Cu}^{\text{II}}\text{Co}^{\text{II}}$ trinuclear system ($S_{\text{Cu}} = 1/2$ and $S_{\text{Co}} = 3/2$). On lowering the temperature, χ_{MT} decreases continuously and reaches $0.2 \text{ cm}^3 \text{ mol}^{-1} \text{ K}$ at 2 K (Fig. 6). On the basis of the

crystal structure of **2**, the magnetic interactions for $\text{Co} \cdots \text{Co}$ through the hpt^{2-} bridges between adjacent tetranuclear $[\text{Co}_2(\text{CuL})(\text{hpt})_2(\text{CH}_3\text{OH})(\text{H}_2\text{O})]$ units can be neglected, because of the larger $\text{Co} \cdots \text{Co}$ separation (about 9.75 Å). Thus, the coupling topology deduced from the crystal structure has to be considered as the CuCo_2 trinuclear unit (shown in Scheme 2). The magnetic analysis was carried out using the spin Hamiltonian: $\hat{H} = -2J_1\hat{S}_{\text{Co}1}\hat{S}_{\text{Co}2} - 2J_2\hat{S}_{\text{Cu}1}\hat{S}_{\text{Co}1} + g\beta\hat{H}_z\hat{S}_z$, where J_1 and J_2 characterize the exchange interactions for $\text{Co} \cdots \text{Co}$ and $\text{Cu} \cdots \text{Co}$, respectively.

To the best of our knowledge, no formula to reproduce the magnetic susceptibility of such a complex system is available in the literature, so we used an approximate way to interpret the magnetic behavior [28,29]. In this model, first we considered Co_2 as a fragment having coupling states of $S = 3, 2, 1, 0$. The populations of each state at various temperatures can be derived as follows:

$$P_3 = \frac{7}{7 + 5 \exp\left(\frac{-6J_1}{kT}\right) + 3 \exp\left(\frac{-10J_1}{kT}\right) + \exp\left(\frac{-12J_1}{kT}\right)} \quad (3)$$

$$P_2 = \frac{5 \exp\left(\frac{-6J_1}{kT}\right)}{7 + 5 \exp\left(\frac{-6J_1}{kT}\right) + 3 \exp\left(\frac{-10J_1}{kT}\right) + \exp\left(\frac{-12J_1}{kT}\right)} \quad (4)$$

$$P_1 = \frac{3 \exp\left(\frac{-10J_1}{kT}\right)}{7 + 5 \exp\left(\frac{-6J_1}{kT}\right) + 3 \exp\left(\frac{-10J_1}{kT}\right) + \exp\left(\frac{-12J_1}{kT}\right)} \quad (5)$$

$$P_0 = \frac{\exp\left(\frac{-12J_1}{kT}\right)}{7 + 5 \exp\left(\frac{-6J_1}{kT}\right) + 3 \exp\left(\frac{-10J_1}{kT}\right) + \exp\left(\frac{-12J_1}{kT}\right)} \quad (6)$$

Second, we evaluated the interactions of the fragment with one $\text{Cu}(\text{II})$ ion. The magnetic susceptibilities of systems containing one $\text{Cu}(\text{II})$ spin and each spin state derived from the central Co_2 cluster can be calculated as follows:

For the 1/2–3 system

$$\chi_3 = \frac{N\beta^2}{4kT} \left[\frac{84g_{7/2}^2 + 35g_{5/2}^2 \exp\left(\frac{-7J_2}{kT}\right)}{4 + 3 \exp\left(\frac{-7J_2}{kT}\right)} \right] \quad (7)$$

$$g_{7/2} = \frac{1}{7}g_{\text{Cu}} + \frac{6}{7}g_{\text{Co}} \quad g_{5/2} = -\frac{1}{7}g_{\text{Cu}} + \frac{8}{7}g_{\text{Co}}$$

For the 1/2–2 system

$$\chi_2 = \frac{N\beta^2}{4kT} \left[\frac{10g_{3/2}^2 + 35g_{5/2}^2 \exp\left(\frac{-5J_2}{kT}\right)}{2 + 3 \exp\left(\frac{-5J_2}{kT}\right)} \right] \quad (8)$$

$$g_{5/2} = \frac{1}{5}g_{\text{Cu}} + \frac{4}{5}g_{\text{Co}} \quad g_{3/2} = -\frac{1}{5}g_{\text{Cu}} + \frac{6}{5}g_{\text{Co}}$$

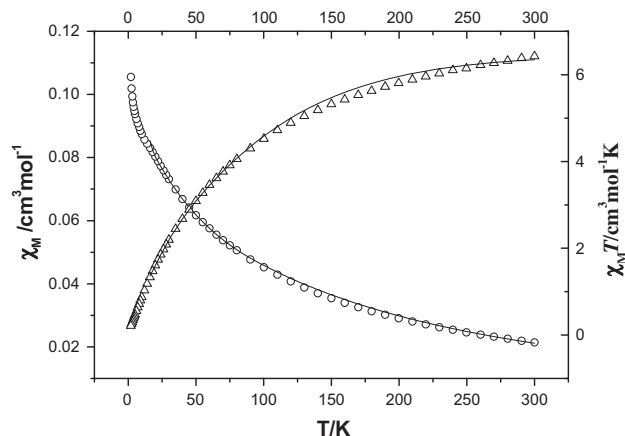
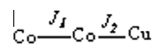


Fig. 6. $\chi_{\text{M}}(O)$ vs. T and $\chi_{\text{MT}}(\Delta)$ vs. T plots for complex **2**.



Scheme 2. The coupling topology deduced from the complex **2**.

For the 1/2–1 system

$$\chi_1 = \frac{N\beta^2}{4kT} \left[\frac{10g_{3/2}^2 + g_{1/2}^2 \exp\left(\frac{-3J_2}{kT}\right)}{2 + \exp\left(\frac{-3J_2}{kT}\right)} \right] \quad (9)$$

$$g_{3/2} = \frac{1}{3}g_{\text{Cu}} + \frac{2}{3}g_{\text{Co}} \quad g_{1/2} = -\frac{1}{3}g_{\text{Cu}} + \frac{4}{3}g_{\text{Co}}$$

For the 1/2–0

$$\chi_0 = \frac{Ng_{\text{Cu}}^2\beta^2}{kT} \frac{1}{2} \left(\frac{1}{2} + 1 \right) \quad (10)$$

Last, the total magnetic susceptibility can be calculated by the following equation:

$$\chi_M = P_3\chi_3 + P_2\chi_2 + P_1\chi_1 + P_0\chi_0 \quad (11)$$

where part of the orbital angular momentum of the Co(II) ion is reflected in the temperature dependence of the g_{Co} factor (Eq. (2)) [27].

The least-squares fit to the experimental data was found with $J_1 = -7.72 \text{ cm}^{-1}$, $J_2 = -7.86 \text{ cm}^{-1}$, $g_{\text{Cu}} = 2.00$ (fixed), $A = 1.20$ and $\lambda = -170 \text{ cm}^{-1}$ (fixed). The agreement factor, defined as $R = \sum [(\chi_M)^{\text{Cal}} - (\chi_M)^{\text{obsd}}]^2 / \sum [(\chi_M)^{\text{obsd}}]^2$, is 1.59×10^{-4} . The point below 16 K cannot be reproduced with this model.

For complex **3**, the $\chi_M T$ value is equal to $6.10 \text{ cm}^3 \text{ mol}^{-1} \text{ K}$ at 300 K, which is larger than the spin-only value ($3.76 \text{ cm}^3 \text{ mol}^{-1} \text{ K}$) expected for the uncoupled Co_2^{II} binuclear system. On lowering the temperature, $\chi_M T$ decreases continuously and reaches $3.02 \text{ cm}^3 \text{ mol}^{-1} \text{ K}$ at 2 K (Fig. S3). Compounds **2** and **3** are isostructural, and the Ni^{II} ion is diamagnetic in the NiL subunit. Thus, the coupling topology deduced from the crystal structure has to be considered as the Co_2 binuclear unit, and the fitting model is the same as for **1**. The least-squares fit to the experimental data was found with $J = -1.78 \times 10^{-2} \text{ cm}^{-1}$, $A = 1.25$ and $\lambda = -140 \text{ cm}^{-1}$. The agreement factor, defined as $R = \sum [(\chi_M)^{\text{Cal}} - (\chi_M)^{\text{obsd}}]^2 / \sum [(\chi_M)^{\text{obsd}}]^2$, is 1.57×10^{-5} . The point below 16 K cannot be reproduced with this model.

For complex **5**, the $\chi_M T$ value is equal to $13.55 \text{ cm}^3 \text{ mol}^{-1} \text{ K}$ at 300 K, which is larger than the spin-only value ($7.50 \text{ cm}^3 \text{ mol}^{-1} \text{ K}$) expected for the uncoupled Co_4^{II} tetranuclear system. On lowering the temperature, $\chi_M T$ decreases continuously and reaches $4.16 \text{ cm}^3 \text{ mol}^{-1} \text{ K}$ at 2 K (Fig. 7). Complex **5** is a one-dimensional ladder-like chain formed by octanuclear $[\text{Co}_4(\text{NiL})_4(\text{ipt})_4(\text{H}_2\text{O})_2]$ units linked by ipt^{2-} ligands. The magnetic interactions for $\text{Co} \cdots \text{Co}$ through the ipt^{2-} bridges between adjacent $[\text{Co}_4(\text{NiL})_4(\text{ipt})_4(\text{H}_2\text{O})_2]$ units can be neglected, because of the larger $\text{Co} \cdots \text{Co}$ separation (about 9.40 \AA). In the $[\text{Co}_4(\text{NiL})_4(\text{ipt})_4(\text{H}_2\text{O})_2]$ unit, the Ni^{II} ion is diamagnetic in the NiL subunit, and the distances between the $\text{Co}1$ or $\text{Co}4$ ion and the center Co_2O_2 cluster are 9.62 or 10.23 \AA , respectively. Thus, for the Co_4Ni_4 unit, the magnetic susceptibility of two cobalt ions is added to that of the Co_2O_2 cluster. For the Co_2O_2 cluster, the magnetic analysis was carried out using the theoretical expression of the magnetic susceptibility deduced from the spin Hamiltonian $\hat{H} = -2J\hat{S}_{\text{Co}2}\hat{S}_{\text{Co}3} + g\beta\hat{H}_z\hat{S}_z$, and the magnetic susceptibility can be calculated from Eq. (1), while the expression of the total magnetic susceptibility was obtained as follows:

$$\chi_M = \chi_{\text{CoCo}} + 2\chi_{\text{Co}}$$

where a part of the orbital angular momentum of the Co(II) ion is reflected in the temperature dependence of the g_{Co} factor (Eq. (2)) [27].

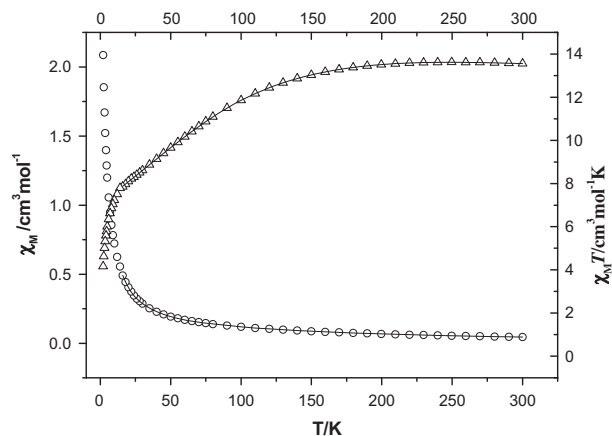


Fig. 7. $\chi_M(O)$ vs. T and $\chi_M T(\Delta)$ vs. T plots for complex **5**.

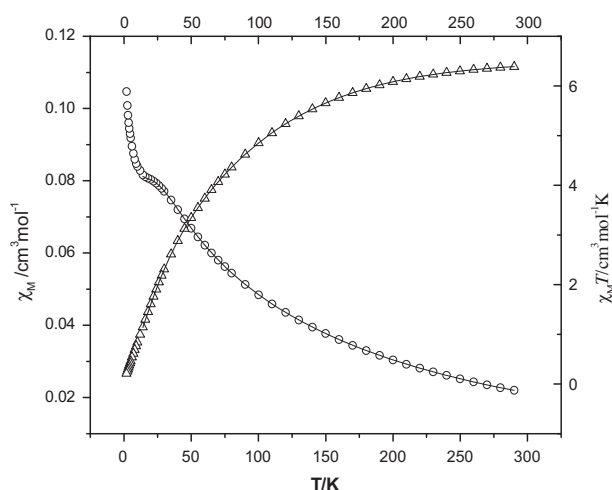
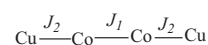


Fig. 8. $\chi_M(O)$ vs. T and $\chi_M T(\Delta)$ vs. T plots for complex **6**.

The least-squares fit to the experimental data was found with $J = -1.10 \times 10^{-2} \text{ cm}^{-1}$, $A = 1.49$ and $\lambda = -120 \text{ cm}^{-1}$. The agreement factor, defined as $R = \sum [(\chi_M)^{\text{Cal}} - (\chi_M)^{\text{obsd}}]^2 / \sum [(\chi_M)^{\text{obsd}}]^2$, is 1.20×10^{-5} . The point below 16 K cannot be reproduced with this model.

The value $\chi_M T = 6.39 \text{ cm}^3 \text{ mol}^{-1} \text{ K}$ at 300 K for a powder sample of **6** is larger than the spin-only value of $6.00 \text{ cm}^3 \text{ mol}^{-1} \text{ K}$ expected for the uncoupled $\text{Cu}_2^{\text{II}}\text{Co}_2^{\text{II}}$ tetranuclear system (Fig. 8). On lowering the temperature, $\chi_M T$ decreases continuously and reaches $0.25 \text{ cm}^3 \text{ mol}^{-1} \text{ K}$ at 2 K. On the basis of the crystal structure of **6**, the magnetic interactions for $\text{Co} \cdots \text{Co}$ through the tpt^{2-} bridges between adjacent tetranuclear $[\text{Co}_2(\text{tpt})_4(\text{CuL})_2]$ units can also be neglected, because of the larger $\text{Co} \cdots \text{Co}$ separation (about 9.96 \AA). Thus, the coupling topology deduced from the crystal structure has to be considered as the Cu_2Co_2 tetranuclear unit (shown in Scheme 3). The magnetic analysis was carried out using the spin Hamiltonian: $\hat{H} = -2J_1\hat{S}_{\text{Co}1}\hat{S}_{\text{Co}1A} - 2J_2(\hat{S}_{\text{Cu}1}\hat{S}_{\text{Co}1} + \hat{S}_{\text{Cu}1A}\hat{S}_{\text{Co}1A}) + g\beta\hat{H}_z\hat{S}_z$, where J_1 and J_2 characterized the exchange interactions for $\text{Co}-\text{Co}$ and $\text{Cu}-\text{Co}$, respectively.

To date, no approximate model for such a system could be used. To estimate a rough exchange constant, we tried to use an



Scheme 3. The coupling topology deduced from the complex **6**.

Table 3

Distances and magnetic information for some coordination polymers containing cobalt(II) with macrocyclic oxamide and aromatic multicarboxylate bridge.

Compound	$d_{\text{Co}\cdots\text{Co}}$ (Å)	$d_{\text{Co}\cdots\text{Cu}}$ (Å)	J_1 (cm^{-1})	J_2 (cm^{-1})	A	λ (cm^{-1})	
1	4.1326		-6.8×10^{-3}		1.49	–120	This work
2	3.1055	5.2930	–7.72	–7.86	1.20	–170 (fixed)	This work
3	3.1499		-1.8×10^{-2}		1.25	–140	This work
5	3.4158		-1.1×10^{-2}		1.49	–120	This work
6	4.3806	5.3870	–2.68	–4.18	1.21	–170 (fixed)	This work
7	3.3467	5.2721	–1.98	–11.88	1.23	–170 (fixed)	Ref. [16]

J_1 and J_2 characterize the exchange interactions for Co–Co (carboxylate bridge) and Cu–Co (oxamide bridge), respectively; and compound **7** is $[\text{Co}(\text{nip})(\text{CuL})(\text{H}_2\text{O})]_n$.

approximate model [28,29,12]. The least-squares fit to the experimental data was found with $J_1 = -2.68 \text{ cm}^{-1}$, $J_2 = -4.18 \text{ cm}^{-1}$, $g_{\text{Cu}} = 2.00$ (fixed), $A = 1.21$ and $\lambda = -170 \text{ cm}^{-1}$ (fixed). The agreement factor, defined as $R = \sum [(\chi_M)^{\text{Cal}} - (\chi_M)^{\text{obsd}}]^2 / \sum [(\chi_M)^{\text{obsd}}]^2$, is 2.10×10^{-6} . The point below 14 K cannot be reproduced with this model.

For complexes **1**, **2**, **3**, **5** and **6**, we used approximate models to estimate the magnetic exchange and spin–orbital interactions for these complexes. The results show that spin–orbit coupling of the Co(II) ion plays an important role in the magnetic behaviors, and the point below 16 K cannot be reproduced with these models, which may be attributed to the zero-field splitting of the Co(II) ion in the $S = 1/2$ state and/or intermolecular interactions. The magnetic information for some coordination polymers containing cobalt(II) ions with macrocyclic oxamide and aromatic multicarboxylate bridges are listed in Table 3. In these complexes the paramagnetic Co^{II} ions bridged by OCO and/or O from carboxylate groups show a weak antiferromagnetic coupling; the J_1 values are -6.80×10^{-3} , -7.72 , -1.78×10^{-2} , -1.10×10^{-2} , -2.68 and -1.98 cm^{-1} . The absolute values can vary depending on ML, the modes of connection, the angles and also on the distance. Of these factors, the electronic effects of ML play an important role in affecting the magnetic exchange between the Co(II) center; it is obvious that $\text{CuL} > \text{NiL}$ (**2**, **6**, **7** \gg **1**, **3**, **5**). For complexes **1**, **3** and **5**, the antiferromagnetic exchange interactions exhibit **3** $>$ **5** $>$ **1**, which can be explained on the basis of the distance and modes of connection. The larger distance and pairwise syn–anti OCO bridging mode in **1** led to a reduction of the overlap integral between the magnetic orbital of Co(II), and resulted in a very small antiferromagnetic coupling constant. For complexes **2**, **6** and **7**, the antiferromagnetic exchange interactions exhibit **2** $>$ **6** $>$ **7**; this can also be rationalized by the distance and modes of connection. In complex **2**, the shorter distance (3.11 Å), syn–syn OCO and O connections between nearest neighbor cobalt(II) ions and the Co–O–Co angle of 89° will mediate relatively stronger antiferromagnetic exchange interactions than those of **6** and **7** (for **6**, Co–Co distance (4.38 Å), pairwise syn–anti OCO bridging mode; for **7**, Co–Co distance (3.35 Å), pairwise O bridging mode and Co–O–Co angle of 97°). Moreover, the electronic effects due to the different aromatic multicarboxylate bridges and molecular topology might affect the magnetic properties.

For complexes **2**, **6** and **7**, the antiferromagnetic interactions through the oxamido group arise from the non-zero overlap between the magnetic orbitals around Cu(II) and Co(II), and the antiferromagnetic exchange interactions exhibit **7** $>$ **2** $>$ **6**. The difference between the magnetic exchanges may be explained on the basis of structural distortions and distances. In this regard, one of the relevant factors is the value of the dihedral angle (γ) between the mean equatorial plane of the metal ion and the oxamido plane [30,31]; the smaller the value of γ , the greater the antiferromagnetic coupling. Complex **7** has a smaller value of γ (13.0) and a shorter Cu–Co distance (5.27 Å), which leads to a greater overlap integral than for **2** and **6** (for **2**, Cu–Co distance (5.29 Å), γ (15.9);

for **6**, Cu–Co distance (5.39 Å), γ (13.7)), and results in a relatively greater antiferromagnetic coupling constant.

4. Conclusions

Six heterometallic coordination polymers containing cobalt(II) were synthesized with macrocyclic oxamide and aromatic multicarboxylate (including aip^{2-} , hpt^{2-} , ipt^{2-} and tpt^{2-}) co-ligands under the same solvothermal reaction conditions. This research reveals that the electronic effects and coordinated modes of different aromatic multicarboxylate ligands play an important role in the structure construction. In one compound, the greater number of different coordinated modes of the multicarboxylate ligands leads to the more complicated and diverse structure. Polymers **2** and **3** hold an unusual two-dimensional framework with nanometric pores, and there are two coordinated modes for the hpt^{2-} ligand. Complex **5** is very novel one-dimensional ladder-like polymer consisting of a Co_4Ni_4 unit, and there are four coordinated modes for the ipt^{2-} ligand in **5**. In complexes **1–6**, although the macrocyclic oxamide complex ML was used as a terminal ligand, the coexistence of macrocyclic oxamide and polycarboxylate bridged-ligands have profound effects on the construction of coordination polymers with different structures and magnetic properties. Complexes **1**, **2**, **3**, **5** and **6** show weak antiferromagnetic exchange interactions between the adjacent metal ions centers, and spin–orbit coupling of Co(II) ion plays an important role in the magnetic behaviors. The magnitude and nature of coupling interactions can be influenced by a series of factors, so investigating the magnetic properties of oxamide and multicarboxylate bridging cores systems is important for further enlightenment of the intimate relationship of spin coupling.

Acknowledgments

This work was supported by the National Natural Science Foundation of China (Nos. 20771083, 20901059, 21001081, 21043004 and 90922032) and the National Basic Research Program of China, 978 Program, 2007CB815305. The Education Commission of Tianjin (No. 20110510) and Tianjin Normal University (No. 52XC1102). Supported by the Program for Innovative Research Team in University of Tianjin.

Appendix A. Supplementary data

CCDC 952581–952586 contains the supplementary crystallographic data for complexes **1–6**. These data can be obtained free of charge via <http://www.ccdc.cam.ac.uk/conts/retrieving.html>, or from the Cambridge Crystallographic Data Centre, 12 Union Road, Cambridge CB2 1EZ, UK; fax: (+44) 1223-336-033; or e-mail: deposit@ccdc.cam.ac.uk. Supplementary data associated with this article can be found, in the online version, at <http://dx.doi.org/10.1016/j.poly.2014.02.035>.

References

- [1] Z.G. Guo, R. Cao, X. Wang, H.F. Li, W.B. Yuan, G.J. Wang, H.H. Wu, J. Li, *J. Am. Chem. Soc.* 131 (2009) 6894.
- [2] M. Yoshizawa, M. Tamura, M. Fujita, *Science* 312 (2006) 251.
- [3] S.L. James, *Chem. Soc. Rev.* 32 (2003) 276.
- [4] N.L. Rosi, J. Eckert, M. Eddaoudi, D.T. Vodak, J. Kim, M. O'Keeffe, O.M. Yaghi, *Science* 300 (2003) 1127.
- [5] S.K. Nune, P.K. Thallapally, A. Dohnalkova, C. Wang, J. Liu, G.J. Exarhos, *Chem. Commun.* 46 (2010) 4878.
- [6] P.K. Thallapally, J. Tian, M.R. Kishan, C.A. Fernandez, S.J. Dalgarno, P.B. McGrail, J.E. Warren, J.L. Atwood, *J. Am. Chem. Soc.* 130 (2008) 16842.
- [7] J.R. Stork, V.S. Thoi, S.M. Cohen, *Inorg. Chem.* 46 (2007) 11213.
- [8] Y. Zhang, B. Chen, F.R. Fronczek, A.W. Maverick, *Inorg. Chem.* 47 (2008) 4433.
- [9] Y.Q. Sun, L.L. Fan, D.Z. Gao, Q.L. Wang, M. Du, D.Z. Liao, C.X. Zhang, *Dalton Trans.* 39 (2010) 9654.
- [10] Y.Q. Sun, L.L. Fan, D.Z. Gao, G.Y. Zhang, *Z. Anorg. Allg. Chem.* 636 (2010) 846.
- [11] Y.Q. Sun, D.Z. Gao, Y.Y. Xu, G.Y. Zhang, L.L. Fan, C.P. Li, T.L. Hu, D.Z. Liao, C.X. Zhang, *Dalton Trans.* 40 (2011) 5528.
- [12] Y.Q. Sun, Y.Y. Xu, D.Z. Gao, G.Y. Zhang, Y.X. Liu, J. Wang, D.Z. Liao, *Dalton Trans.* 41 (2012) 5704.
- [13] E. Coronado, J.R. Galán-Mascarós, C.J. Gómez-García, V. Laukhin, *Nature* 408 (2000) 447.
- [14] C.P. Berlinguette, A. Dragulescu-Andrasi, A. Sieber, J.R. Galán-Mascarós, H.U. Gudel, C. Achim, K.R. Dunbar, *J. Am. Chem. Soc.* 126 (2004) 6222.
- [15] M. Murre, *Chem. Soc. Rev.* 39 (2010) 1986.
- [16] G.E. Kostakis, S.P. Perlepes, V.A. Blatov, D.M. Proserpio, A.K. Powell, *Coord. Chem. Rev.* 256 (2012) 1246.
- [17] P.K. Chen, Y.X. Che, J.M. Zheng, S.R. Batten, *Chem. Mater.* 10 (2007) 2162.
- [18] S.D. Han, W.C. Song, J.P. Zhao, Q. Yang, S.J. Liu, Y. Li, X.H. Bu, *Chem. Commun.* 49 (2013) 871.
- [19] Y. Oka, K. Inoue, H. Kumagai, M. Kurmoo, *Inorg. Chem.* 52 (2013) 2142.
- [20] J.P. Zhao, Q. Yang, Z.Y. Liu, R. Zhao, B.W. Hu, M. Du, Z. Chang, X.H. Bu, *Chem. Commun.* 48 (2012) 6568.
- [21] E. Pardo, R.R. Garcia, F. Lloret, J. Faus, M. Julve, Y. Journaux, F. Delgado, C.R. Perez, *Adv. Mater.* 16 (2004) 1597.
- [22] D.S.C. Black, H. Corrie, *Inorg. Nucl. Chem. Lett.* 12 (1976) 65.
- [23] P.W. Selwood, *Magnetochemistry*, Interscience, New York, 1956. p. 78.
- [24] F. Lloret, Y. Journaux, M. Julve, *Inorg. Chem.* 29 (1990) 3967.
- [25] K. Nakamoto, *Infrared and Raman Spectra of Inorganic and Coordination Compounds*, fifth ed., John Wiley, New York, 1997. Part B.
- [26] H. Akashi, N. Uryū, T. Shibahara, *Inorg. Chim. Acta* 53 (1997) 261.
- [27] F. Lloret, M. Julve, J. Cano, R. Ruiz-García, E. Pardo, *Inorg. Chim. Acta* 361 (2008) 3432.
- [28] Z.L. Liu, L.C. Li, L. Zhang, D.Z. Liao, Z.H. Jiang, S.P. Yan, *New J. Chem.* 27 (2003) 583.
- [29] H.Z. Kou, B.C. Zhou, D.Z. Liao, R.J. Wang, Y.D. Li, *Inorg. Chem.* 41 (2002) 6887.
- [30] S. Alvarez, M. Julve, M. Verdaguier, *Inorg. Chem.* 29 (1990) 4500.
- [31] J.L. Sanz, B. Cervera, R. Ruiz, C. Bois, J. Faus, F. Lloret, M. Julve, *J. Chem. Soc., Dalton Trans.* 7 (1996) 1359.